photonics

MDPI

Article

Performance and Compatibility Evaluation of Uniform, Apodized, and Titled Fiber Bragg Grating Profiles with New HMT-Enhanced SnO_2 Coating for Optical-Based Humidity Sensing Improvement

Soo Ping Kok [1], Yun Ii Go [1,*], Siti Barirah Ahmad Anas [2] and M. L. Dennis Wong [3,4]

[1] School of Engineering and Physical Sciences, Heriot-Watt University Malaysia, Putrajaya 62200, Malaysia; k.ping@hw.ac.uk
[2] Wireless and Photonics Networks Research Centre, Faculty of Engineering, Universiti Putra Malaysia, Serdang 43400, Malaysia
[3] School of Engineering, Newcastle University, Newcastle upon Tyne NE1 7RU, UK
[4] Newcastle University Medicine Malaysia, Educity, Iskandar Puteri 79200, Malaysia
* Correspondence: y.go@hw.ac.uk

Abstract

Optical-based sensors have been widely used for various applications, including biosensing, civil structural health monitoring, and humidity sensing. Fiber Bragg Grating (FBG) is one of the optical-based sensing approaches that are commonly used in these applications. The effect of hygroscopic coating on different grating profiles, including uniform, apodized, and tilted FBG, was investigated by connecting the FBG to a light source and optical spectrum analyzer (OSA). The reflected wavelength of the FBG, captured by the OSA at increasing and decreasing relative humidity ranging from 40 to 80% RH were recorded. Tin dioxide (SnO_2) is one of the metal oxides with a hygroscopic nature, which is suitable to act as a coating material for FBG. For improved sensitivity, the HMT-enhanced technique was applied in this study to modify the surface morphology of SnO_2, increasing the porosity of the nanostructure for water adsorption and desorption. The result showed that the sensitivity and linearity of the FBG-based humidity sensor can be enhanced via HMT-enhanced SnO_2 nanostructure coating onto uniform FBG. A sensitivity of 1.30 pm/%RH and 1.52 pm/%RH was reported during incremental and decremental RH, respectively, and a fitting coefficient of >0.97 was recorded. This approach demonstrated the feasibility of hygroscopic coating on FBG to enable broad applications across various humidity sensing industries such as agriculture, pharmaceutical, and semiconductors.

Keywords: OSA; wavelength shift; sensitivity; spectral; refractive index; hygroscopic

Check for updates

Received: 23 December 2025
Revised: 30 January 2026
Accepted: 9 February 2026
Published: 11 February 2026

1. Introduction

Fiber Bragg Grating (FBG) is one of the optical fiber sensors in which the diffraction grating causes the refractive index undergo quasi-periodic modulation along the fiber core [1,2]. The grating structure within the fiber core reflects a specific narrow band of wavelength, called the Bragg wavelength, and transmits the remaining wavelength with minimal attenuation, as illustrated in Figure 1 [3]. The central wavelength of FBG, according to the coupled-mode theory (CMT), is given by the following [4]:

$$\lambda_B = 2n_{eff}\Lambda \quad (1)$$

where λ_B is the Bragg wavelength, n_{eff} is the effective refractive index, and Λ is the grating period.

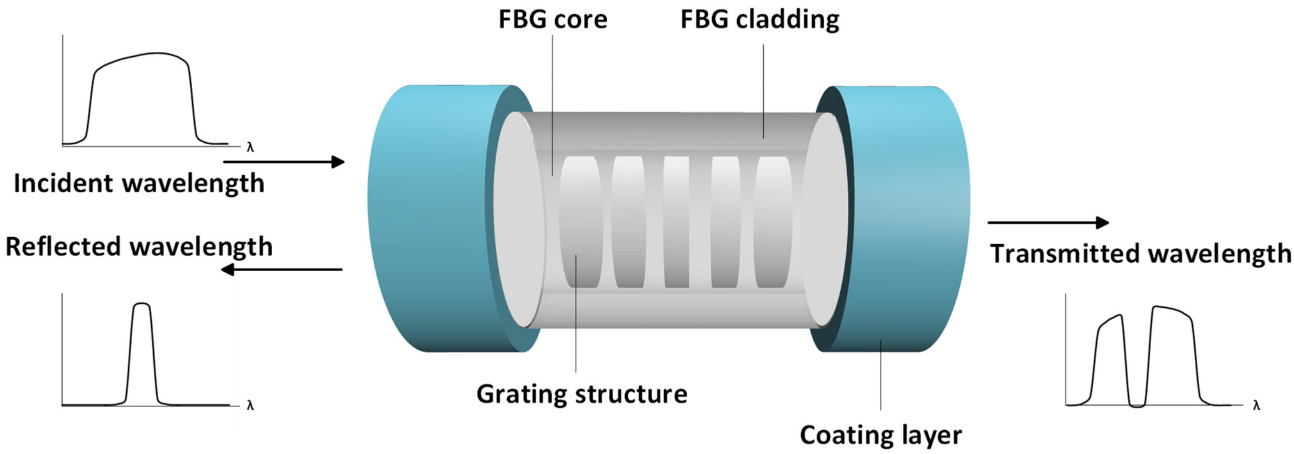

Figure 1. Conceptual illustration of uniform FBG, adapted from [5].

Uniform FBG refers to contradirectional coupling waveguides with a constant period, phase, and amplitude along their length [5,6]. The CMT stated the transmittance, T, and reflectance, R, characteristics of a uniform FBG, given by the following [7]:

$$T = 1 - R \tag{2}$$

$$R = tanh^2 \kappa L \tag{3}$$

where κ is the coupling coefficient, and L is the grating length.

The propagation constant, β, of a contradirectional coupling waveguide is expressed as follows [7]:

$$\beta_1 = -\beta_2 = \kappa n_{eff} \tag{4}$$

The reflected wavelength of FBG is usually caused by the change in refractive index induced by the change in physical parameters such as temperature, T, and strain, ε, leading to the shift in central wavelength, which is expressed as follows [8]:

$$\Delta\lambda_B = \lambda_B (K_T \Delta T + K_\varepsilon \Delta\varepsilon) \tag{5}$$

where K_T is the temperature sensitivity, and K_ε is the strain sensitivity.

Apodized FBG shows advantages of minimizing side-lobe in the reflection spectrum, as the change in refractive index is reduced gradually towards the edge of the grating structure [9]. The grating profile also allows optimization of optical characteristics, including reflectivity and FWHM.

The reflectivity of a function of grating length L and wavelength λ of apodized FBG, using CMT, is given as follows [10]:

$$R\,(L,\,\lambda) = \frac{\kappa^2 sinh^2(sL)}{s^2 cosh^2(sL) + \Delta\beta^2 sinh^2(sL)} \tag{6}$$

where Δβ is the differential propagating constant given as β = β − β_0. The β and β_0 are given as follows:

$$\beta = \frac{2\pi n_0}{\lambda} \tag{7}$$

$$\beta_0 = \frac{\pi}{\Lambda} \tag{8}$$

https://doi.org/10.3390/photonics13020178

$$s^2 = \kappa^2 - \Delta\beta^2 \tag{9}$$

The grating structure of tilted FBG is usually slanted at an angle of around 4 to 30°, which allows the cladding mode to be adjusted according to the perturbation for response optimization [11]. The tilted FBG measures the transmission spectrum for sensing purposes as a collection of backward-propagating cladding mode resonances [12]. The resonant wavelength based on phase matching condition is given by the following [13]:

$$\lambda_{core} = \frac{2n_{eff}^{co}\Lambda}{\cos\theta} \tag{10}$$

$$\lambda_{cl} = \frac{n_{eff}^{cl} + n_{eff}^{co}\Lambda}{\cos\theta} \tag{11}$$

where λ_{co} and λ_{cl} are the wavelength of the core and cladding mode, and n_{eff}^{co} and n_{eff}^{cl} are the effective mode indices of λ_{co} and λ_{cl}, respectively. θ represents the tilted angle of the grating structure.

The transmittance of a tilted FBG is expressed as follows [13]:

$$T = 1 - tanh^2(\kappa L) \tag{12}$$

FBG is usually designed for the purposes of telecommunication owing to its capability in suppressing the birefringence in conventional SMF [14]. Other common applications of FBG are temperature and strain sensing, where the wavelength shifts induced by the refractive index perturbation are detected with high precision [15,16]. To enable humidity sensing, hygroscopic materials such as polyimides, graphene oxide, and metal oxides have been explored for FBG coating [17,18]. These materials exhibit advantages such as good sensitivity, linearity, and thermal stability to realize high-performance humidity sensors [19,20]. Previous studies have been carried out on polyimide-coated FBG and reported a sensitivity of 1.5 pm/%RH and a fitting coefficient of ~0.99 within a humidity range of 11 to 83% RH [21]. Another research was conducted on polyimide coated on micro-nano uniform FBG, fabricated via a tapering process [2]. A sensitivity of 0.8 pm/%RH and a fitting coefficient of 0.982 were reported during decremental RH from 65 to 30% RH. A tilted FBG with polyvinyl alcohol (PVA) and graphene oxide (GO) coating revealed sensitivity of −0.24 pm/%RH from 35 to 85% RH [22].

Limited studies reported the performance of apodized and tilted grating profiles. Although the hygroscopicity of metal oxides has been explored previously, their coating on FBG has not been extensively studied. One of the metal oxides, tin dioxide (SnO_2), has gained attention due to its chemical and physical stability [23]. However, this material often showed limitations when exposed to high humidity levels [24]. Modification on SnO_2, such as doping, nanocomposite, and additive-enhanced technique have also been investigated to increase the humidity sensing performance of the hygroscopic materials [25–27]. A Zn-doped SnO_2 nanoparticle showed improved response time compared to pure SnO_2 within a humidity range from 11 to 97% RH, contributed by the doping technique that results in the formation of cauliflower-like morphology with enhanced porosity and formation of oxygen vacancies [25].

The tungsten disulfide (WS_2)-modified SnO_2 hybrid nanocomposite revealed an improved sensing response of 8.5 and 862.8 times higher than pure SnO_2 and WS_2, respectively [26]. The nanocomposite technique created synergistic effects between SnO_2 and WS_2, increasing specific surface area, preventing the agglomeration between SnO_2, and providing more active sites for water adsorption. The HMT increases the porosity and surface area of SnO_2, improving the water uptake of the nanostructure, which is dominated by pore surface adsorption [28]. The material properties lead to enhanced hygroscopic strain around three to four times over the same RH interval, which increases the swelling effect on the fiber core when coated onto the FBG sensing region [29]. Among all the improvement techniques, coating of HMT-enhanced SnO_2 onto FBG has yet to be examined. Therefore, this study will focus on the coating of the proposed nanostructure onto FBG with different grating profiles.

2. Materials and Methods

The experiments started with FBG sample fabrication, followed by FBG preparation and the drop casting method to coat the hygroscopic material onto the FBG sensing region. The surface of the coated material was tested to understand the morphology formation, whereas the optical performance was examined through the change in the FBG reflected spectrum. The overall process flow was illustrated in Figures 2–4.

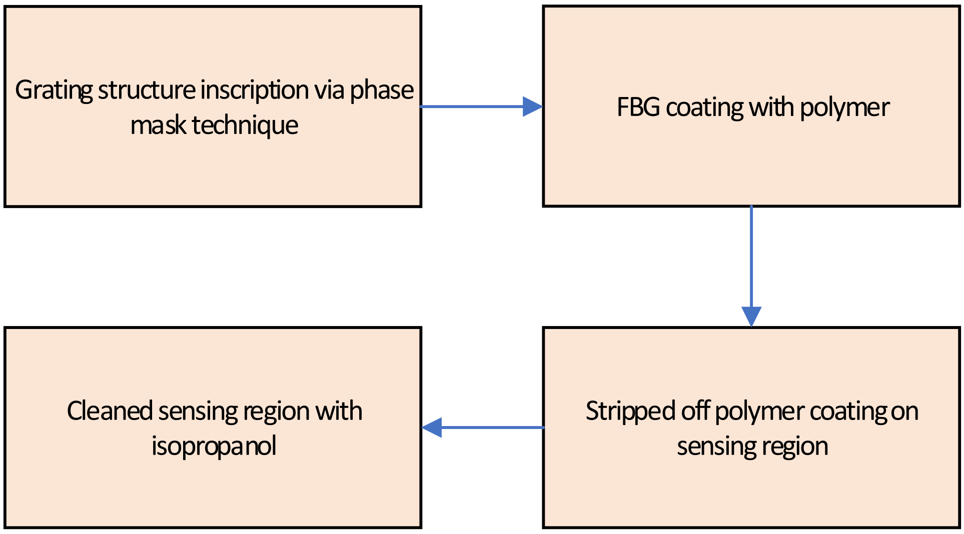

Figure 2. Process flow chart for FBG fabrication and preparation stage.

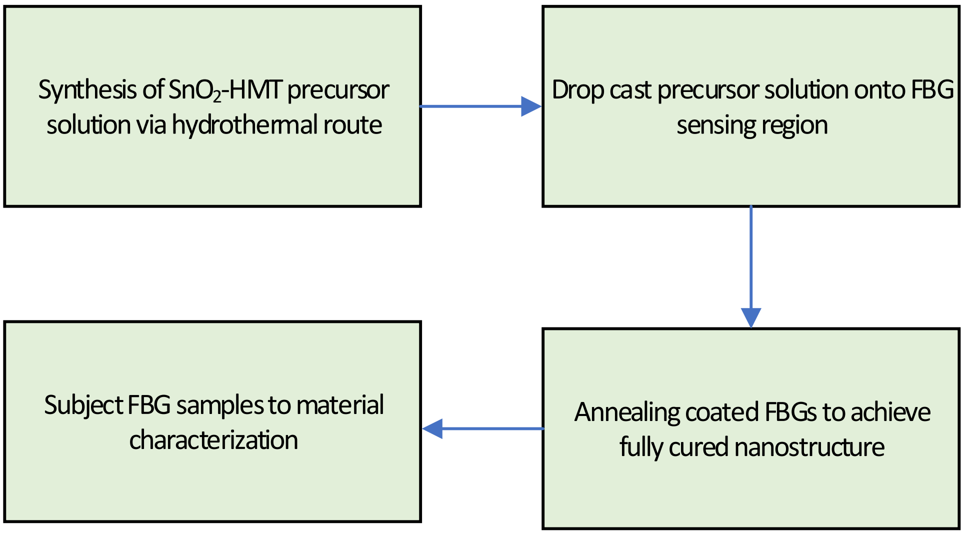

Figure 3. Process flow chart for hygroscopic coating and material characterization stage.

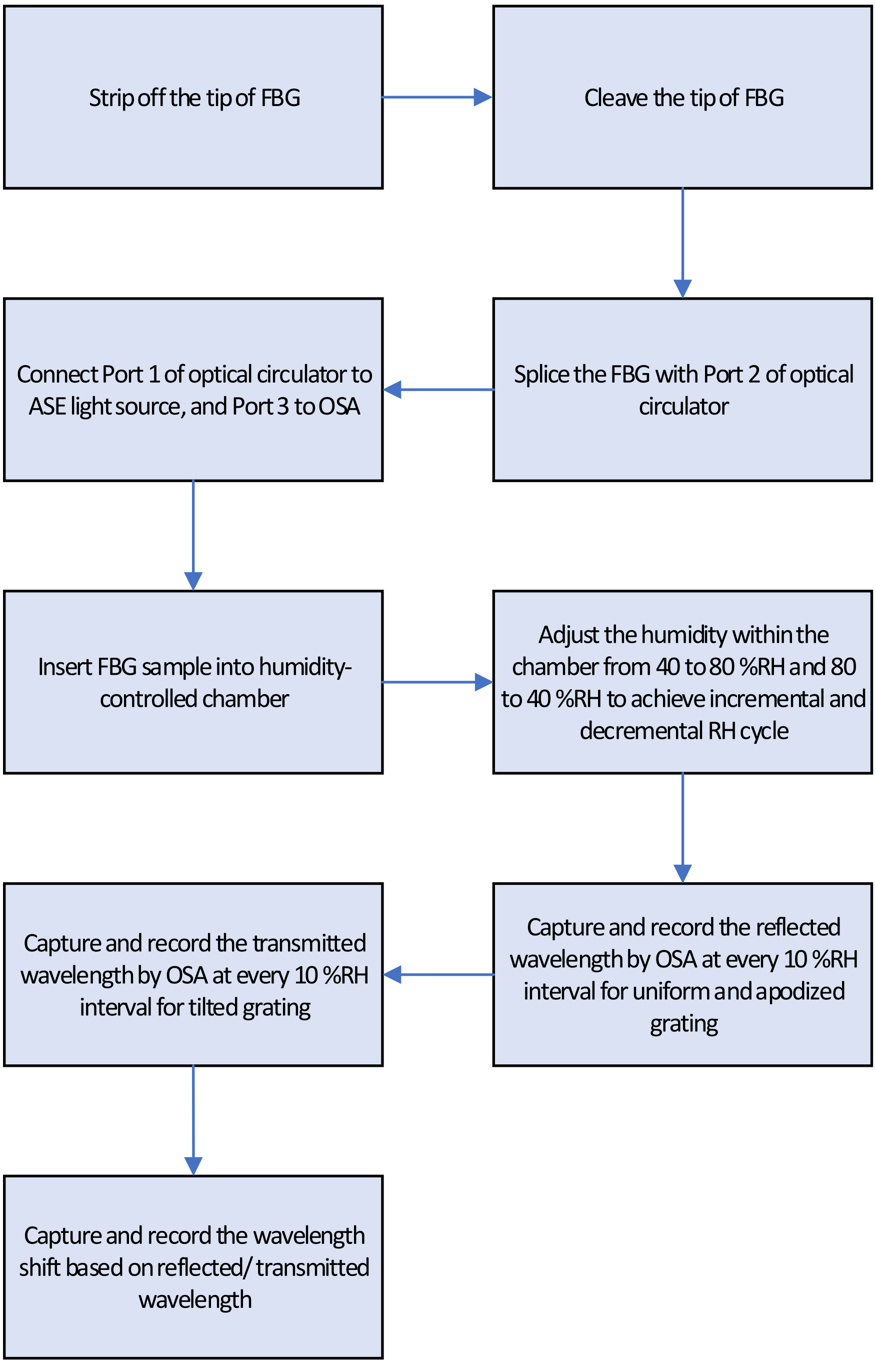

Figure 4. Process flow chart for optical spectrum analysis stage.

2.1. FBG Fabrication and Preparation Stage

The FBG samples were fabricated via the phase mask technique [30], based on the unique properties of the ultraviolet-sensitive characteristic of single-mode optical fiber, as illustrated in Figure 5. Three grating profiles were selected as uniform grating is most applied across broad applications, including humidity sensing, apodized grating offers side-lobe suppression [31], and tilted grating offers self-compensation while enabling multiparameter sensing [13].

To inscribe the grating structure onto the core of an uncoated FBG via a writing platform, the phase mask was placed between the UV light and the targeted FBG to incur a periodic interference pattern along the fiber. For an apodized grating, a uniform phase mask and a Gaussian beam laser were applied for the fabrication, whereas the tilted grating was fabricated by rotating the phase mask and FBG to the desired angle relative to the UV beam.

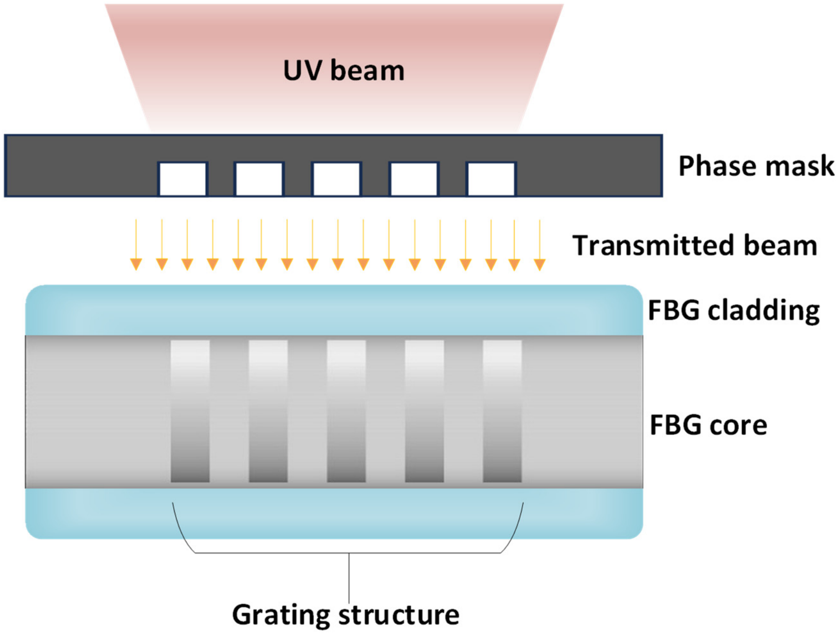

Figure 5. Conceptual illustration of uniform FBG fabrication.

Upon inscription, the FBG was coated with a polymer coating and cured under a thermal-controlled environment. The fabrication process yields FBGs with different grating structures with the listed specifications, as shown in Table 1. To prepare the FBG for hygroscopic coating, the polymer coating of the FBG sensing region was stripped off using a fiber stripper and cleaned with isopropanol to ensure no residue remains on the cladding surface.

Table 1. FBG specification of different grating profiles.

Grating Profile	Specification
Uniform	FBG CW: 1540 nm +/−0.5 nm FBG Length: 10 mm BW@3 dB: 0.25+/−0.05 nm Ref > 80%
Apodized	FBG CW: 1550 nm +/−0.5 nm FBG Length: 10 mm BW@3 dB: 0.25+/−0.05 nm Ref > 80% SLSR > 15 db
Tilted	Angle: 5° FBG CW: 1550 nm +/−0.5 nm FBG Length: 10 mm BW@3 dB: 0.3+/−0.1 nm Ref > 70%

2.2. Hygroscopic Coating and Material Characterization Stage

The HMT-enhanced SnO_2 coating solution, which was prepared via a low-temperature hydrothermal route [32], was coated onto the sensing region using a drop casting technique [33]. To ensure uniformity of coating, the FBG was placed on a hotplate heated to 80 °C, and 100 µL of coating solution was dropped onto the sensing region and let dry for

1 min using a micropipette. The same steps were repeated until 500 µL of coating solution was coated to fully cover the surroundings of the sensing region.

Upon coating, the FBG was subject to annealing at 140 °C for 3 h, to ensure the precursor was fully cured on the FBG surface. The same preparation and coating steps were repeated for FBG with different grating profiles. For the analysis of mass change in hygroscopic material, a modified gravimetric technique was carried out in a sealed humidity-controlled chamber for the hygroscopicity test. This technique was selected as the water uptake is dominated by adsorption on internal pore surfaces rather than bulk lattice expansion.

The RH levels within the chamber were adjusted incrementally from 40 to 80% RH, and decrementally from 80 to 40% RH. The mass change in the material at every 10% RH was measured and recorded. To understand the surface morphology of hygroscopic material coated onto FBG, a Field Emission Scanning Electron Microscope (FESEM) was used on the coated region, whereas Energy-Dispersive X-ray Spectroscopy (EDS) was carried out to verify the chemical elemental composition of the coated SnO_2-HMT.

2.3. Optical Spectrum Analysis Stage

To capture the reflected wavelength of FBG under different RH levels of uniform and apodized grating, one end of the coated FBG was connected to the optical circulator (port 2). One end of the optical circulator (port 1) was connected to the ASE light source for light input, and port 3 was connected to the optical spectrum analyzer (OSA), as illustrated in Figure 6. For the tilted grating, the setup was illustrated in Figure 7, where the optical circulator was removed, and one end of the FBG was connected to the ASE light source and OSA, respectively. Fiber stripping, cleaving, and splicing have been carried out on the FBG and optical circulator to enable signal transmission.

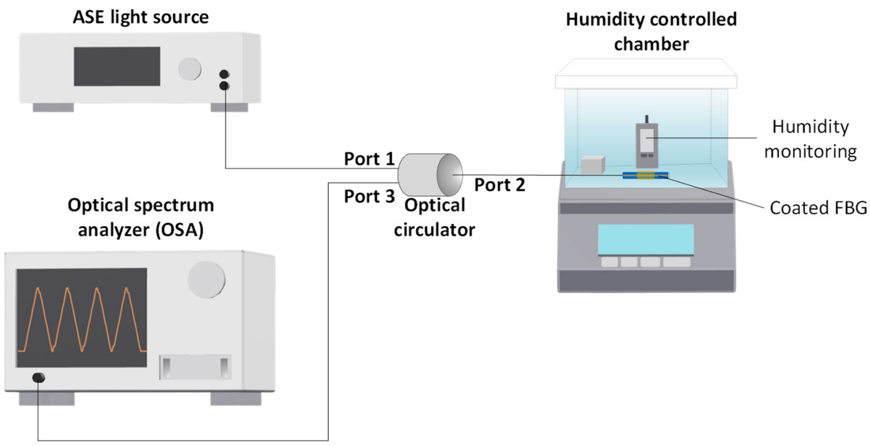

Figure 6. Schematic diagram of laboratory setup for uniform and apodized grating.

The coated FBG was placed into a sealed humidity-controlled chamber, with the same setup as the hygroscopicity test. All four FBG grating profiles coated with SnO_2-HMT were tested under the same humidity conditions, and the optical spectrum analysis was conducted. The FBG samples were connected to the same setup of light source and OSA equipment. The reflected wavelength or transmitted wavelength captured by the OSA was recorded at every 10% RH. For uniform and apodized grating, the wavelength shift was recorded based on the reflected wavelength of the fiber core [34], as illustrated in Figure 8, whereas the wavelength shift in tilted grating was recorded based on the transmitted wavelength corresponding to core modes, as the core modes reflection is effective in normalize the sensor's response [35,36], as shown in Figure 9.

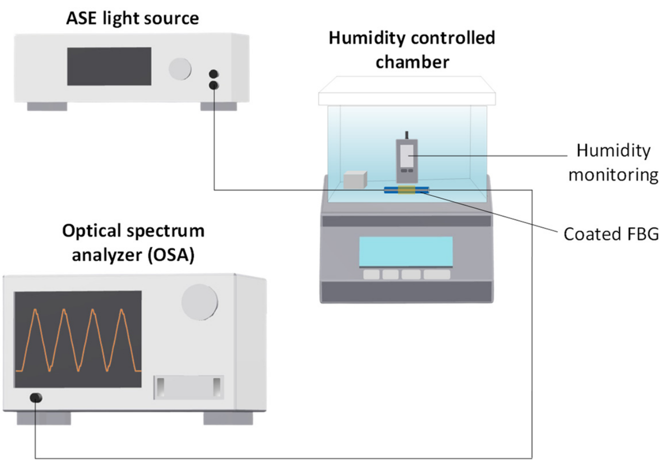

Figure 7. Schematic diagram of laboratory setup for tilted grating.

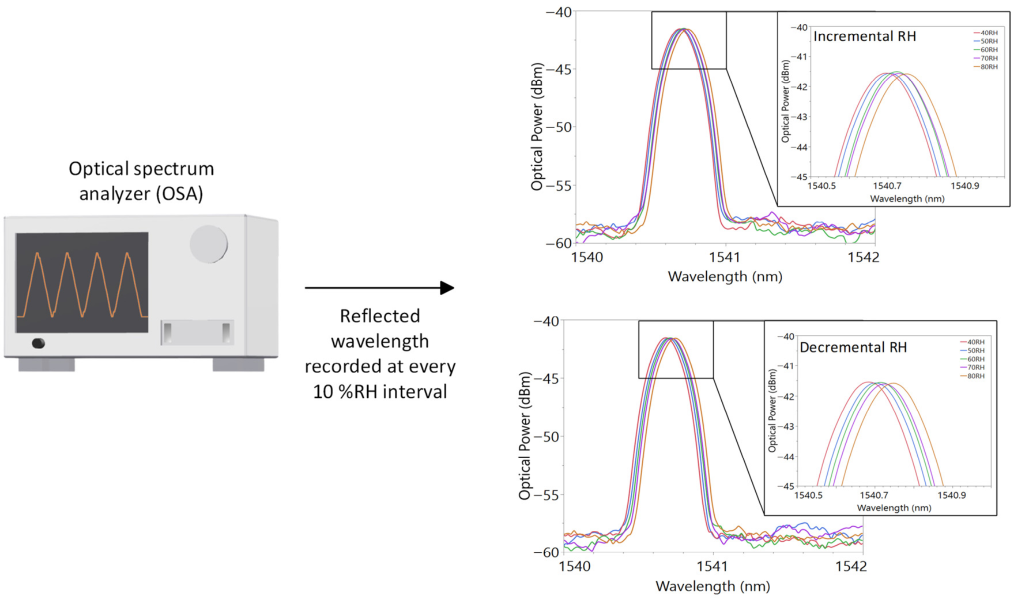

Figure 8. Reflected wavelength of uniform FBG obtained from OSA at every 10% RH interval.

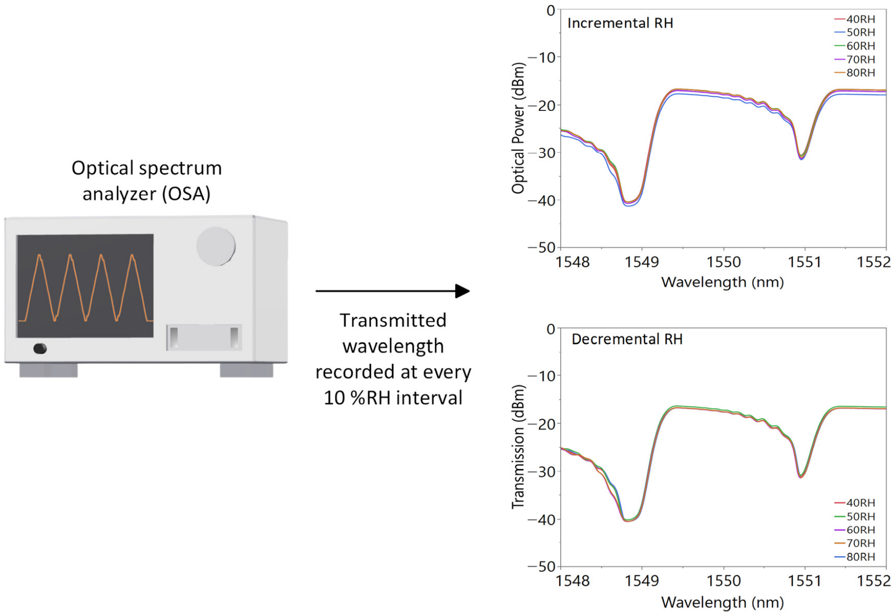

Figure 9. Transmitted wavelength of tilted FBG obtained from OSA at every 10% RH interval.

3. Result and Discussion

3.1. Hygroscopicity Test

The hygroscopicity test was conducted on SnO_2-HMT, and the mass change at every 10% RH interval was listed in Table 2. A slope coefficient of 0.11 and a fitting coefficient of >0.96 was obtained from the linear regression of mass change over RH. The mass uptake ratio was also calculated based on the oven-dried material mass, and a slope coefficient of 0.16 was recorded from the linear regression of mass uptake ratio over RH.

Table 2. Mass changes in SnO_2-HMT under incremental and decremental RH cycle.

Relative Humidity (%RH)	Mass (mg), Incremental RH	Mass (mg), Decremental RH
40	71.97	72.17
50	72.53	72.70
60	74.47	74.80
70	75.30	75.40
80	76.30	76.30

3.2. Material Characterization

An FESEM image under 100× magnification was captured on the uniform FBG coated with SnO_2-HMT, and EDS was performed on the coated surface for the analysis of elemental composition, as shown in Figure 10. FESEM image under 30,000× magnification, as shown in Figure 11, indicated the formation of SnO_2-HMT nanoparticle surrounding the FBG sensing region. The tin (Sn) and oxygen (O) elements observed from the EDS were attributed to the SnO_2 coating material, whereas the carbon (C) element was caused by the presence of HMT, one of the organic surfactants. Minor chloride (Cl) residue can be observed from the EDS, as the coating solution is being prepared using a precursor of tin (ii) chloride dihydrate ($SnCl_2{\cdot}2H_2O$) under a low-temperature hydrothermal route. Since the hygroscopicity of SnO_2-HMT is dominated by the porous structure, a minimum trace of Cl residues does not significantly alter pore surface adsorption or swelling characteristics.

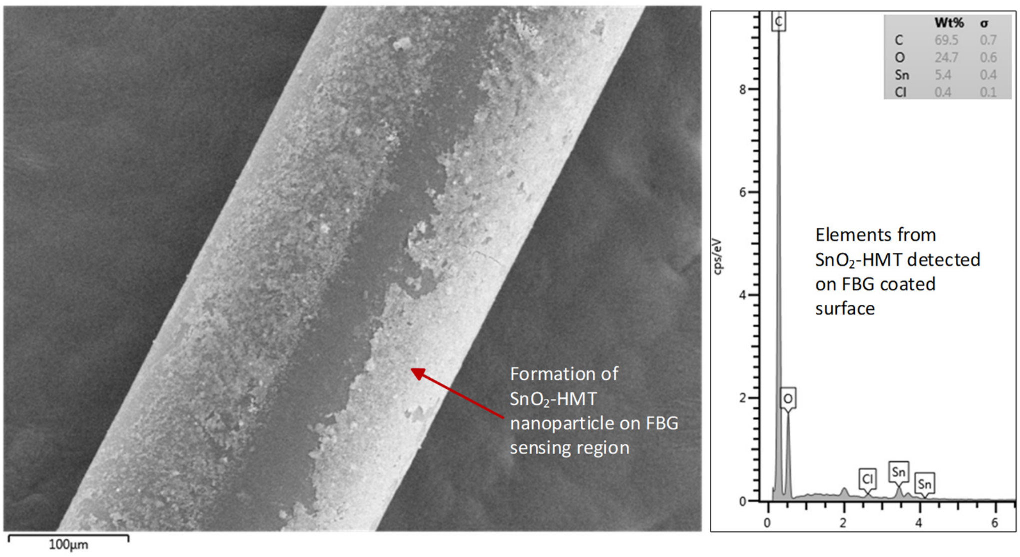

Figure 10. FESEM and EDS of coated FBG under 100× magnification.

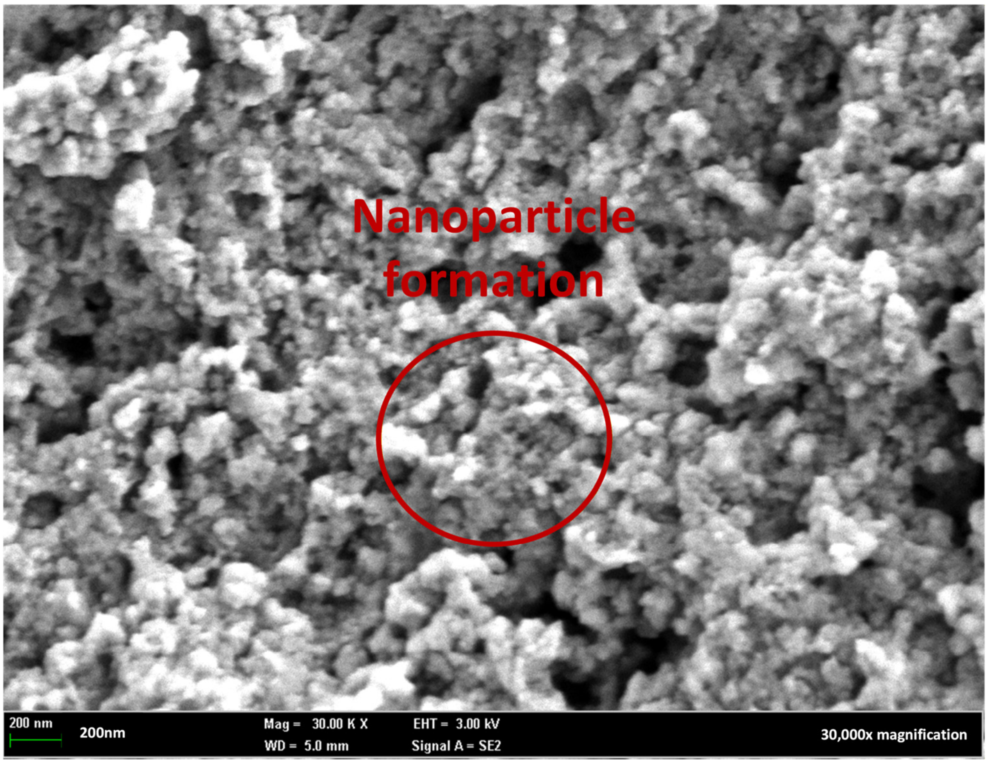

Figure 11. FESEM of coated FBG under 30,000× magnification.

The cross-sectional view of coated SnO_2-HMT from FESEM image under 150× magnification, as shown in Figure 12, revealed that no delamination between the coating material and substrate occurred upon exposure to incremental and decremental humidity cycles. The coating thickness was approximately 55–57 μm.

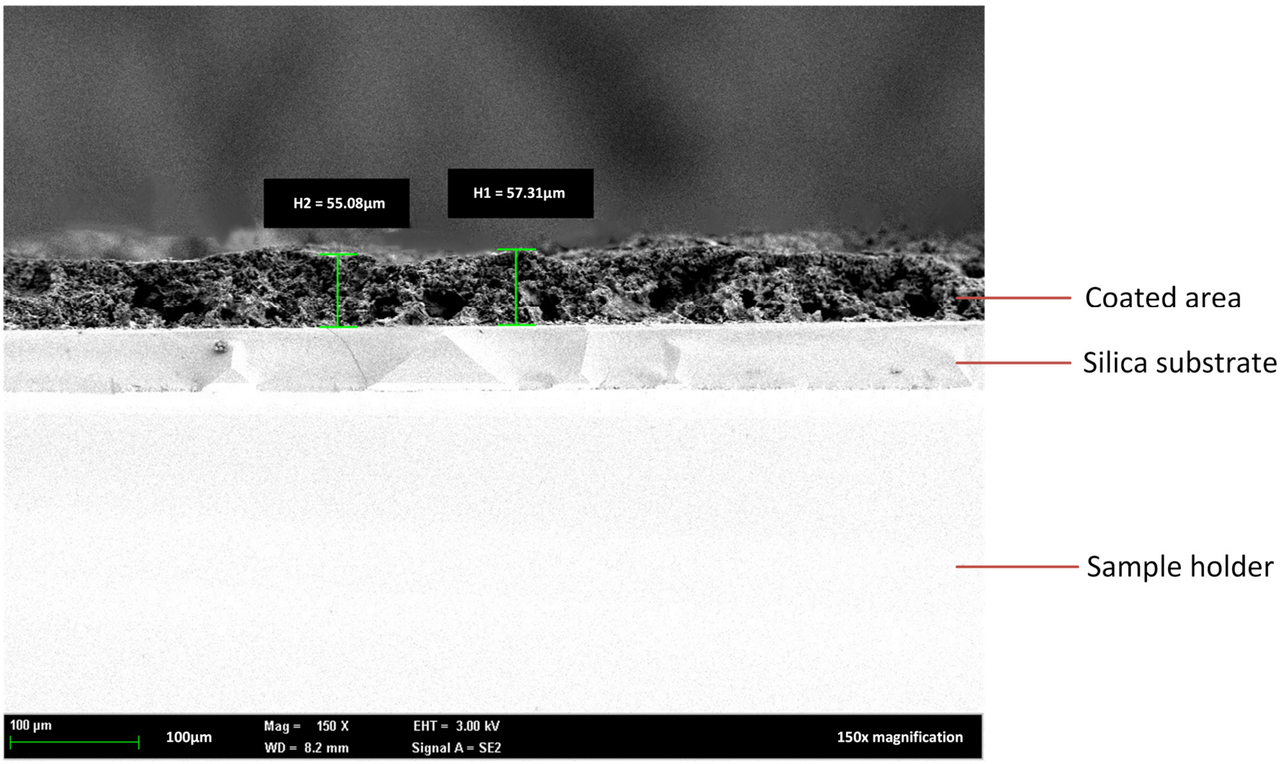

Figure 12. FESEM of SnO_2-HMT cross-sectional view under 150× magnification.

3.3. Optical Spectrum Analysis

The linear equation (y = mx + c) of the wavelength shift has been calculated as illustrated in Figures 13–15. Comparing the three different grating profiles as illustrated in Table 3, the uniform grating showed the highest sensitivity, which is 1.30 pm/%RH during incremental RH, and 1.52 pm/%RH during decremental RH. The uniform grating also showed the highest linear fitting coefficient compared to other samples, where the R^2 value is >0.97. The sensitivity of the apodized and tilted grating is <0.5 pm/%RH when subject to a humidity cycle under the same conditions, where the apodized grating showed the lowest R^2 value with <0.9. The time elapsed for each 10% RH interval is shown in Figure 16. A 15 min waiting time was applied to record the wavelength change for each incremental and decremental change of 10% RH.

Table 3. Optical spectrum analysis of different grating profiles.

Grating Profile	Incremental RH			Decremental RH		
	%RH	Reflected Wavelength (nm)	Sensitivity (pm/% RH)	%RH	Reflected Wavelength (nm)	Sensitivity (pm/% RH)
Uniform	40	1540.694	1.30	80	1540.748	1.52
	50	1540.706		70	1540.725	
	60	1540.723		60	1540.714	
	70	1540.728		50	1540.701	
	80	1540.748		40	1540.684	
Apodized	40	1550.666	0.34	80	1550.681	0.42
	50	1550.670		70	1550.668	
	60	1550.670		60	1550.668	
	70	1550.674		50	1550.664	
	80	1550.681		40	1550.662	
Tilted	40	1548.828	0.26	80	1548.840	0.44
	50	1548.831		70	1548.834	
	60	1548.834		60	1548.826	
	70	1548.833		50	1548.824	
	80	1548.840		40	1548.823	

The uniform grating provides a consistent grating profile along the core, improving the interaction between evanescent fields with the hygroscopic coating and increasing sensor sensitivity and linearity. The lower effective refractive index modulation towards the edge of the apodized grating could reduce the effect of hygroscopic coating along the sensing region [37], whereas the cladding mode of tilted grating was more sensitive to external perturbation, leading to the lower sensitivity and linearity of the FBGs in humidity sensing applications [38].

The hysteresis of incremental and decremental is calculated by the following [25]:

$$Hysteresis\ \% = \frac{\Delta Y}{\Delta Y_{span}} \times 100 \quad (13)$$

where ΔY is the maximum and minimum value of wavelength at maximum hysteresis, and ΔY_{span} is the maximum and minimum values of wavelength in the humidity range of 40–80% RH.

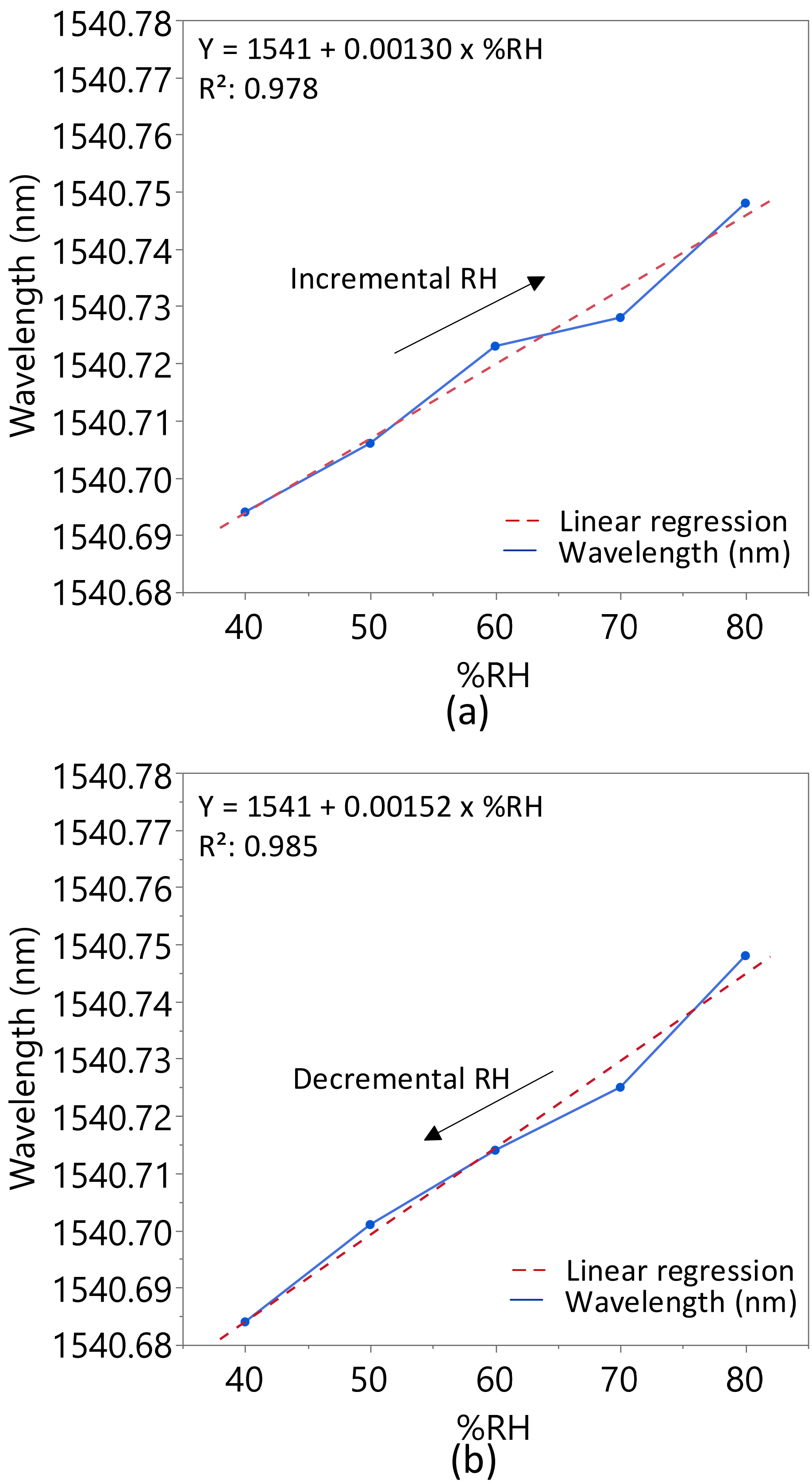

Figure 13. Wavelength shift in uniform grating under (**a**) incremental RH and (**b**) decremental RH.

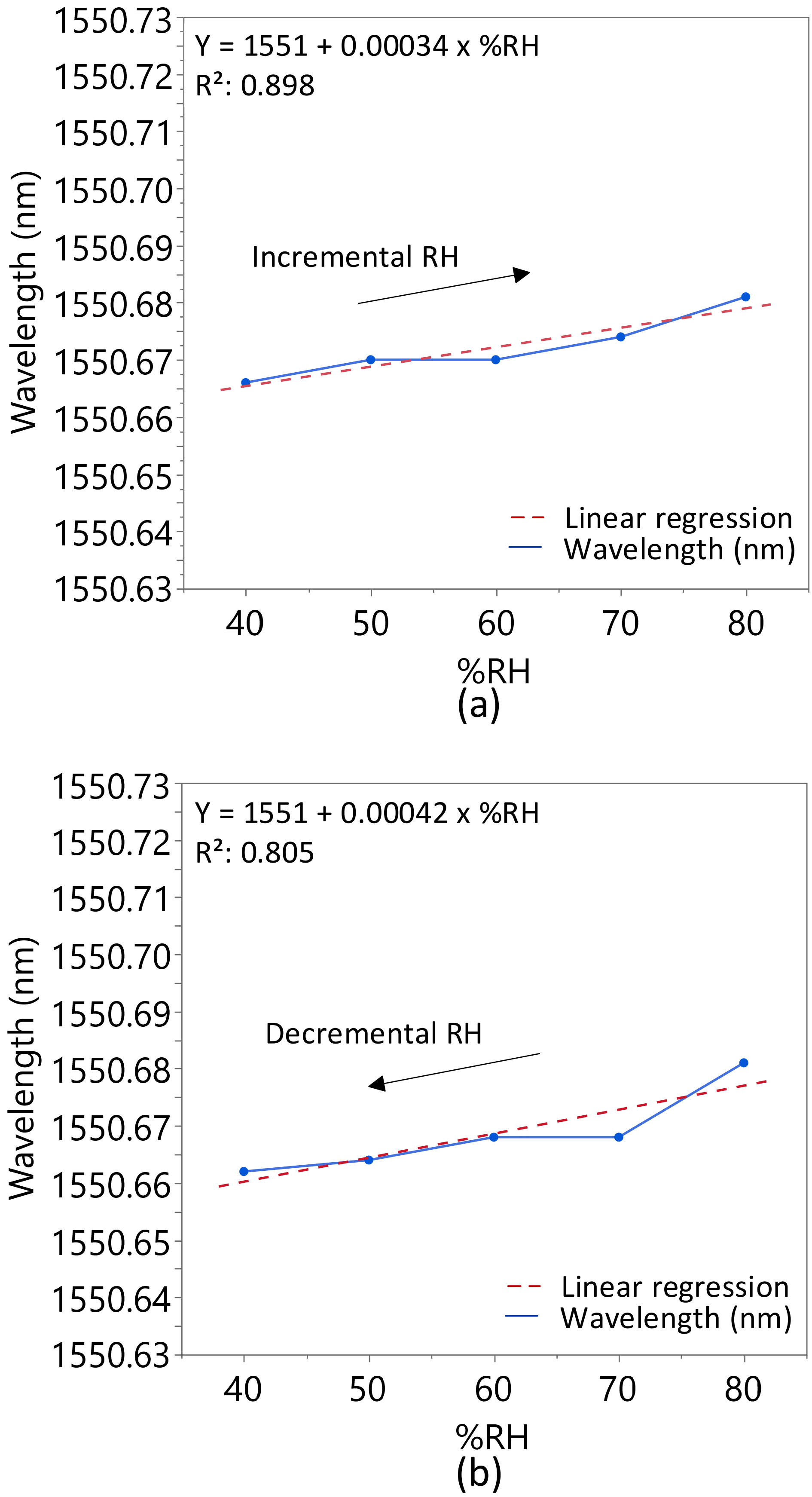

Figure 14. Wavelength shift in apodized grating under (**a**) incremental RH and (**b**) decremental RH.

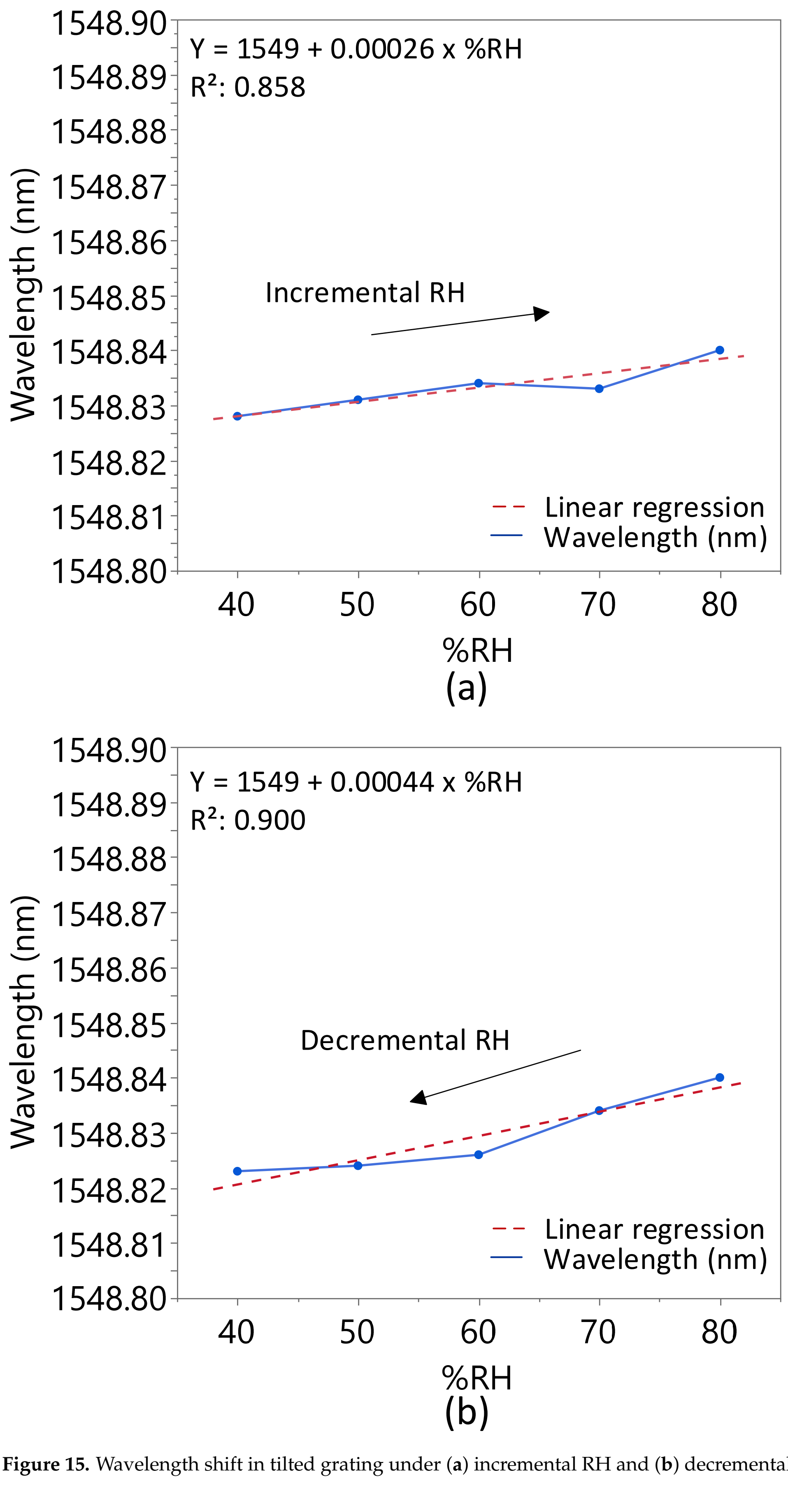

Figure 15. Wavelength shift in tilted grating under (**a**) incremental RH and (**b**) decremental RH.

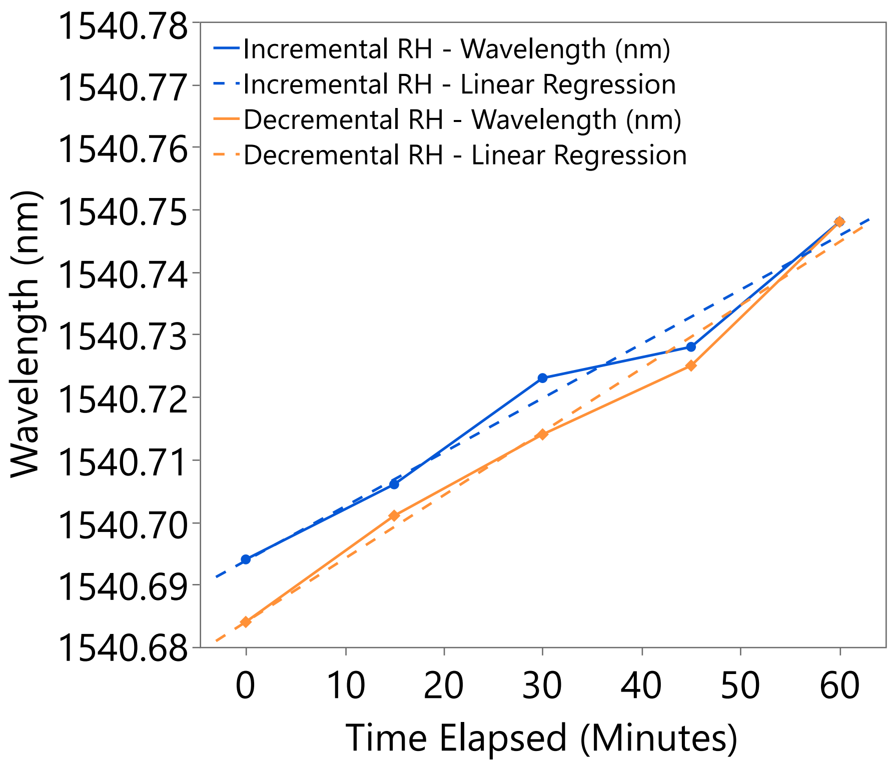

Figure 16. Time elapsed of uniform grating under incremental RH and decremental RH.

For uniform grating, the maximum hysteresis calculated at 40% RH was 16%. At high humidity levels, the hysteresis dropped to 4% and 2% at 70% RH and 80% RH, respectively, indicating the water desorption started to slow down at lower humidity levels. This can be attributed to the uniform moisture-induced swelling effect of the coating materials dominating the FBG strain change at higher humidity levels. However, during desorption, the shrinkage of the coating material did not transfer back to the sensing region with the same efficiency, due to limited interfacial adhesion.

Despite the highest sensitivity and linearity of the uniform grating in this study, apodized and tilted grating offer advantages in other sensing applications. The side-lobe suppression in apodized grating enables long-distance monitoring applications [34]. The capability to excite the cladding mode of tilted grating improves interaction with the surrounding medium [39]. Although the uniform grating showed improved performance in humidity sensing, the apodized grating can be deployed for cascaded FBG sensing network in wavelength division multiplexing systems [40], whereas the tilted grating is suitable for simultaneous sensing in biosensing or chemical sensing applications [41,42].

4. Conclusions

This paper evaluated the performance of uniform, apodized, and tilted FBG in humidity sensing and reported a sensitivity of 1.30, 0.34, and 0.26 pm/% RH, respectively, under incremental RH, and 1.52, 0.42, and 0.44 pm/%RH, respectively, under decremental RH. The study also revealed the highest linearity in uniform FBG, with R^2 values of 0.978 and 0.985, respectively, for incremental and decremental RH, which outperform both apodized and tilted grating with an R^2 value below 0.9.

This result showed coating of SnO_2-HMT enabled an increase in sensitivity and linearity of uniform grating compared to apodized and tilted grating, which can be due to the compatibility between the hygroscopic coating and uniform grating structure, leading to consistent strain change throughout the incremental and decremental RH cycle. The overall low sensitivity can be due to the coating-substrate adhesion being slightly weaker, jeopardizing the effective transfer of the swelling effect to the FBG axial sensing region [43]. The narrow spectra of apodized grating contribute to side-lobe suppression, with a tradeoff of reduced effective refractive index modulation along the sensing region, limiting the sensitivity toward refractive index perturbation induced by water–surface interaction. The tilted grating exhibited advantages in core-cladding mode coupling but increased the susceptibility to environmental interference.

However, both apodized and tilted grating own advantages in other applications, including high-speed transmission systems with dispersion compensation and sensor networks for long-distance monitoring using apodized FBG [34,44], and simultaneous measurement of multiple parameters such as temperature, strain, and liquid level with tilted FBG [45,46]. For continuous improvement of FBG in humidity sensing performance, especially for increased sensitivity, surface preparation, such as etching, can be further explored to enhance the adhesion between coating materials and substrate [47]. Another approach is to introduce an adhesion layer between the coating material and the substrate for improved interfacial contact, reducing the mechanical loss to achieve higher sensitivity [43].

Author Contributions: Conceptualization, S.P.K.; Methodology, S.P.K.; Validation, S.P.K.; Formal Analysis, S.P.K.; Investigation, S.P.K.; Resources, S.B.A.A.; Data Curation, S.P.K.; Writing—Original Draft, S.P.K.; Writing—Review and Editing, Y.I.G.; Visualization, S.P.K.; Supervision, Y.I.G.; Project Administration, Y.I.G.; Funding Acquisition, Y.I.G. and M.L.D.W. All authors have read and agreed to the published version of the manuscript.

Funding: This work was supported by the Ministry of Higher Education Malaysia through the Fundamental Research Grant Scheme (FRGS) under Grant FRGS/1/2023/TK08/HWUM/02/2.

Data Availability Statement: Data is contained within the article.

Conflicts of Interest: The authors declare no conflicts of interest.

References

1. Lin, R.; Lei, M.; Ding, S.; Cheng, Q.; Ma, Z.; Wang, L.; Tang, Z.; Zhou, B.; Zhou, Y. Applications of flexible electronics related to cardiocerebral vascular system. *Mater. Today Bio* **2023**, *23*, 100787. [CrossRef]
2. Li, P.; Yan, H.; Xie, Z.; Zhao, X.; Han, D. A bandwidth response humidity sensor with micro-nano fibre Bragg grating. *Opt. Fiber Technol.* **2019**, *53*, 101998. [CrossRef]
3. Riza, M.A.; Go, Y.I.; Harun, S.W.; Maier, R.R. FBG sensors for environmental and biochemical applications—A review. *IEEE Sens. J.* **2020**, *20*, 7614–7627. [CrossRef]
4. Min, R.; Liu, Z.; Pereira, L.; Yang, C.; Sui, Q.; Marques, C. Optical fiber sensing for marine environment and marine structural health monitoring: A review. *Opt. Laser Technol.* **2021**, *140*, 107082. [CrossRef]
5. Bernier, M.; Talbot, L.; Boilard, T.; Pleau, L.-P.; Fuerbach, A.; Bharathan, G.; Ams, M. Chapter 4—Fiber Bragg gratings in soft glass fibers. In *Mid-Infrared Fiber Photonics*; Jackson, S., Bernier, M., Vallée, R., Eds.; Woodhead Publishing: Cambridge, UK, 2022; pp. 179–231.
6. Kok, S.P.; Go, Y.I.; Xu, W.; Wong, M.D. Advances in Fibre Bragg Grating (FBG) Sensing: A Review of Conventional and New Approaches and Novel Sensing Materials in Harsh and Emerging Industrial Sensing. *IEEE Sens. J.* **2024**, *24*, 29485–29505. [CrossRef]
7. Okamoto, K. Chapter 4—Coupled Mode Theory. In *Fundamentals of Optical Waveguides*, 3rd ed.; Okamoto, K., Ed.; Academic Press: Cambridge, MA, USA, 2022; pp. 169–217.
8. Liu, H.-l.; Zhu, Z.-w.; Zheng, Y.; Liu, B.; Xiao, F. Experimental study on an FBG strain sensor. *Opt. Fiber Technol.* **2018**, *40*, 144–151. [CrossRef]
9. Mohammed, N.A.; Ali, T.A.; Aly, M.H.; Member, O. Evaluation and performance enhancement for accurate FBG temperature sensor measurement with different apodization profiles in single and quasi-distributed DWDM systems. *Opt. Lasers Eng.* **2014**, *55*, 22–34. [CrossRef]
10. Chaoui, F.; Aghzout, O.; Chakkour, M.; El Yakhloufi, M. Apodization Optimization of FBG Strain Sensor for Quasi-Distributed Sensing Measurement Applications. *Act. Passiv. Electron. Compon.* **2016**, *2016*, 6523046. [CrossRef]
11. Guo, T.; Liu, F.; Guan, B.-O.; Albert, J. Tilted fiber grating mechanical and biochemical sensors. *Opt. Laser Technol.* **2016**, *78*, 19–33. [CrossRef]

12. Korganbayev, S.; Sypabekova, M.; Amantayeva, A.; González-Vila, Á.; Caucheteur, C.; Saccomandi, P.; Tosi, D. Optimization of cladding diameter for refractive index sensing in tilted fiber Bragg gratings. *Sensors* **2022**, *22*, 2259. [CrossRef]
13. Ren, Z.; Huang, Z.; Wang, F.; Wu, J.; Zhou, J.; Wang, Z.; Zhang, Y.; Wang, Z.; Dong, J.; Liu, D. Tilted fiber Bragg grating surface plasmon resonance based optical fiber cadmium ion trace detection. *Sens. Actuators B* **2023**, *393*, 134247. [CrossRef]
14. Yang, S.; Zhang, Q.; Yang, L.; Liu, H.; Wang, Q.; Zhang, P.; Shen, H.; Li, Y. Optomechanical sensor network with fiber Bragg gratings. *Nat. Commun.* **2025**, *16*, 10795. [CrossRef] [PubMed]
15. Hamarsheh, M.M.; Jazar, A.A.; Eltaif, T. Athermally packaged fiber Bragg grating for sensor and DWDM applications using liquid carbon. *Heliyon* **2025**, *11*, e44120. [CrossRef]
16. Riza, M.A.; Go, Y.I.; Zaitizila, I.; Kok, S.P. A Review of Advanced Reactive Materials in Fiber Sensor Technology: Challenges and Requirements of Precise Humidity Control in Mechanochemical Treatment Process. *Sens. Mater.* **2025**, *37*, 41–61. [CrossRef]
17. Wang, W.; Sun, T.; Peng, J.; Dai, J.; Yang, M. Humidity Sensor Based on Fiber BraggGratingCoated With DifferentPore-FoamingAgentDopedPolyimides. *IEEE Photonics Technol. Lett.* **2017**, *29*, 1963–1966. [CrossRef]
18. Wang, Y.; Shen, C.; Lou, W.; Shentu, F.; Zhong, C.; Dong, X.; Tong, L. Fiber optic relative humidity sensor based on the tilted fiber Bragg grating coated with graphene oxide. *Appl. Phys. Lett.* **2016**, *109*, 031107. [CrossRef]
19. Kapic, A.; Tsirou, A.; Verdini, P.G.; Carrara, S. Humidity sensors for high energy physics applications: A review. *IEEE Sens. J.* **2020**, *20*, 10335–10344. [CrossRef]
20. Riza, M.A.; Go, Y.I.; Maier, R.R.; Harun, S.W.; Anas, S.B. Hygroscopic materials and characterization techniques for fiber sensing applications: A review. *Sens. Mater.* **2020**, *32*, 3755–3772. [CrossRef]
21. Zhang, J.; Shen, X.; Qian, M.; Xiang, Z.; Hu, X. An optical fiber sensor based on polyimide coated fiber Bragg grating for measurement of relative humidity. *Opt. Fiber Technol.* **2021**, *61*, 102406. [CrossRef]
22. Deng, L.; Sun, H.; Xi, J.; Yang, Y.; Liu, X.; Jian, C.; Li, X.; Li, J. Simulation and Experiment of Tilted Fiber Bragg Grating Humidity Sensor Coated with PVA/GO Nanofiber Films by Electrospinning. *Sensors* **2025**, *25*, 7386. [CrossRef] [PubMed]
23. Habibzadeh, S.; Kazemi-Beydokhti, A.; Khodadadi, A.A.; Mortazavi, Y.; Omanovic, S.; Shariat-Niassar, M. Stability and thermal conductivity of nanofluids of tin dioxide synthesized via microwave-induced combustion route. *Chem. Eng. J.* **2010**, *156*, 471–478. [CrossRef]
24. Suematsu, K.; Sasaki, M.; Ma, N.; Yuasa, M.; Shimanoe, K. Antimony-doped tin dioxide gas sensors exhibiting high stability in the sensitivity to humidity changes. *ACS Sens.* **2016**, *1*, 913–920. [CrossRef]
25. Basavanagoudra, H.; Jangannanavar, V.D.; Anegundi, S.; Basavalingappa, C.; Patil, M.K.; Inamdar, S.R.; Goudar, K.M. Nanoscopic hygrometry: Exploiting porous nature zinc-doped tin oxide nanoparticles for enhanced humidity sensing at ambient temperature. *Sens. Actuators A* **2024**, *370*, 115242. [CrossRef]
26. Chen, Y.; Pei, Y.; Jiang, Z.; Shi, Z.; Xu, J.; Wu, D.; Xu, T.; Tian, Y.; Wang, X.; Li, X. Humidity sensing properties of the hydrothermally synthesized WS_2-modified SnO_2 hybrid nanocomposite. *Appl. Surf. Sci.* **2018**, *447*, 325–330. [CrossRef]
27. Kok, S.P.; Go, Y.I.; Anas, S.B.A.; Dennis Wong, M.; Chan, K.Y. Additive-Enhanced SnO_2 FBG Sensor with Optimized Annealing Time, Temperature, and Multilayer Coating for High-Performance Humidity Sensing. *Nanomaterials* **2025**, *15*, 1508. [CrossRef]
28. Kok, S.P.; Go, Y.I.; Wong, M.L.D. Effect of Hygroscopic and Electronic Materials, Challenges, and Sensing Requirements in Humidity-Controlled Industry. *J. Electron. Mater.* **2025**, *54*, 6960–6981. [CrossRef]
29. Smagin, A.V.; Sadovnikova, N.B. Hygroscopy as an Indicator of Specific Surface Area in Polymer Materials. *Polymers* **2024**, *16*, 593. [CrossRef]
30. Habel, J.; Boilard, T.; Frenière, J.-S.; Trépanier, F.; Bernier, M. Femtosecond FBG written through the coating for sensing applications. *Sensors* **2017**, *17*, 2519. [CrossRef] [PubMed]
31. Yang, C.; Lai, Y. Apodised fiber Bragg gratings fabricated with a uniform phase mask using Gaussian beam laser. *Opt. Laser Technol.* **2000**, *32*, 307–310. [CrossRef]
32. Riza, M.A.; Go, Y.I.; Maier, R.R.; Harun, S.W.; Anas, S.B.A. Hygroscopicity enhancement of low temperature hydrothermally synthesized zinc oxide nanostructure with heterocyclic organic compound for humidity sensitization. *Sens. Actuators B* **2021**, *345*, 130010. [CrossRef]
33. Kok, S.P.; Go, Y.I.; Xu, W.; Wong, M.D. A Review of Nanostructure Coating Techniques to Achieve High-Precision Optical Fiber Sensing Applications. *Nanomanufacturing* **2024**, *4*, 214–240. [CrossRef]
34. Braunfelds, J.; Haritonovs, E.; Senkans, U.; Kurbatska, I.; Murans, I.; Porins, J.; Spolitis, S. Designing of Fiber Bragg Gratings for Long-Distance Optical Fiber Sensing Networks. *Model. Simul. Eng.* **2022**, *2022*, 8331485. [CrossRef]
35. Tomyshev, K.; Dolzhenko, E.I.; Golubev, I.D.; Butov, O.V. Spectral features of tilted fiber bragg gratings inscribed with femtosecond-pulse laser radiation. *IEEE Sens. J.* **2024**, *24*, 38996–39001. [CrossRef]
36. Guo, T.; Ivanov, A.; Chen, C.; Albert, J. Temperature-independent tilted fiber grating vibration sensor based on cladding-core recoupling. *Opt. Lett.* **2008**, *33*, 1004–1006. [CrossRef]
37. Maiti, S.; Singh, V. Performance analysis of apodized fiber Bragg gratings for sensing applications. *Silicon* **2022**, *14*, 581–587. [CrossRef]

38. Zhang, Z.; Liu, K.; Jiang, J.; Xu, T.; Wang, S.; Ma, J.; Chang, P.; Zhang, J.; Liu, T. Refractometric sensitivity enhancement of weakly tilted fiber Bragg grating integrated with black phosphorus. *Nanomaterials* **2020**, *10*, 1423. [CrossRef] [PubMed]
39. Ooi, C.-W.; Udos, W.; Lim, K.-S.; Wei, H.; Yang, H.; Ahmad, H. Insights and perspectives on modal characteristics in tilted fiber Bragg gratings: A review. *IEEE Sens. J.* **2024**, *24*, 36247–36260. [CrossRef]
40. Mustafa, F.M.; Sayed, A.F.; Aly, M.H. A reduced power budget and enhanced performance in a WDM system: A new FBG apodization function. *Opt. Quantum Electron.* **2022**, *54*, 471. [CrossRef]
41. Sypabekova, M.; Korganbayev, S.; González-Vila, Á.; Caucheteur, C.; Shaimerdenova, M.; Ayupova, T.; Bekmurzayeva, A.; Vangelista, L.; Tosi, D. Functionalized etched tilted fiber Bragg grating aptasensor for label-free protein detection. *Biosens. Bioelectron.* **2019**, *146*, 111765. [CrossRef]
42. Singh, Y.; Raghuwanshi, S.K.; Prakash, O.; Saini, P.K. Design and development of tilted fiber Bragg grating (TFBG) chemical sensor with regression analysis of grating parameters for sensitivity optimization. *Opt. Quantum Electron.* **2021**, *53*, 664. [CrossRef]
43. Maier, C.; Egger, L.; Köck, A.; Reichmann, K. Investigation of the Influence of Adhesion Layers on the Gas Sensing Performance of CuO/Cu_2O Thin Films. *Chemosensors* **2025**, *13*, 80. [CrossRef]
44. Dar, A.B.; Jha, R.K. Chromatic dispersion compensation techniques and characterization of fiber Bragg grating for dispersion compensation. *Opt. Quantum Electron.* **2017**, *49*, 108. [CrossRef]
45. Kipriksiz, S.E.; Yücel, M. Tilted fiber Bragg grating design for a simultaneous measurement of temperature and strain. *Opt. Quantum Electron.* **2021**, *53*, 6. [CrossRef]
46. Osuch, T.; Jurek, T.; Markowski, K.; Jedrzejewski, K. Simultaneous measurement of liquid level and temperature using tilted fiber Bragg grating. *IEEE Sens. J.* **2015**, *16*, 1205–1209. [CrossRef]
47. Vendittozzi, C.; Di Micco, E.; Caponero, M.A.; D'Amato, R. Functional Coatings for Fiber Bragg Gratings: A Critical Review of Deposition Techniques for Embedded and Harsh-Environment Applications. *Coatings* **2025**, *15*, 1268. [CrossRef]